Functional Nanoparticles

DOI: 10.1002/anie.201100884

Tunable, Ultrasensitive pH-Responsive Nanoparticles Targeting Specific Endocytic Organelles in Living Cells**

*Kejin Zhou, Yiguang Wang, Xiaonan Huang, Katherine Luby-Phelps, Baran D. Sumer, and Jinming Gao**

In recent years, multifunctional nanoparticles have received considerable attention in many applications such as biosensors, diagnostic nanoprobes, and targeted drug delivery.[1] These efforts have been driven to a large extent by the need to improve biological specificity in diagnosis and therapy through the precise spatiotemporal control of agent delivery. To achieve this goal, continuous efforts have been dedicated to the development of stimuli-responsive nanoplatforms.[2] Environmental stimuli that were exploited include pH,[3] temperature,[4] enzymatic expression,[5] redox reaction,[6] and light.[7] Among these activating signals, pH triggers belong to the most extensively studied stimuli based on two types of differences in pH: a) pathological (e.g. tumor) versus normal tissues and b) acidic intracellular compartments.[8] For example, owing to the unusual acidity of the tumor extracellular microenvironment ($pH_e \approx 6.5$), several pH_e-responsive nanosystems were reported to increase the sensitivity of tumor imaging or the efficacy of therapy.[9]

To target the acidic endosomal/lysosomal compartments, nanovectors with pH-cleavable linkers were reported to improve payload bioavailability.[10] Furthermore, several smart nanovectors with pH-induced charge conversion were designed to increase drug efficacy.[11] Despite these remarkable advances, specific transport and activation of nanoparticles in different endocytic organelles during endocytosis in living cells is not well documented.[12] The endocytic system comprises a series of compartments that have distinct roles in the sorting, processing, and degradation of internalized cargo. Selective targeting of different endocytic compartments by pH-sensitive nanoparticles is challenging owing to the short nanoparticle residence times (on the order of minutes) and small pH differences in these compartments (e.g. less than 1 pH unit between early endosomes and lysosomes).[13]

Herein we report a set of tunable, pH-activatable micellar (pHAM) nanoparticles based on the supramolecular self-assembly of ionizable block copolymer micelles (Figure 1).

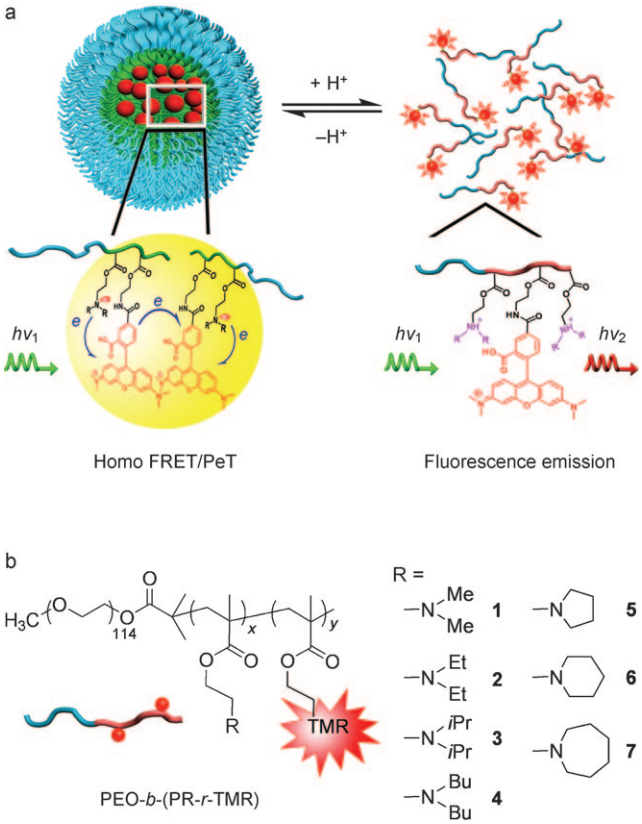

Figure 1. a) Schematic design of pH-activatable micellar (pHAM) nanoprobes. At $pH > pK_a$ of ammonium groups (left panel), the neutralized PR segments self-assemble into the micelle cores, leading to quenching of fluorophores by homoFRET and PeT mechanisms. Upon pH activation ($pH < pK_a$, right panel), formation of charged ammonium groups results in micelle dissociation into unimers with a dramatic increase in fluorescence emission. b) Structures of the PEO-*b*-(PR-*r*-TMR) copolymers in the dialkyl and cyclic series. FRET = Förster resonance energy transfer, PeT = photoinduced electron transfer, PEO = poly(ethylene oxide), PR = ionizable block, TMR = tetramethyl rhodamine.

[*] Dr. K. Zhou,[+] Dr. Y. Wang,[+] Dr. X. Huang,[+] Prof. J. Gao
Department of Pharmacology
Simmons Comprehensive Cancer Center
UT Southwestern Medical Center at Dallas
5323 Harry Hines Blvd, Dallas, TX 75390 (USA)
Fax: (+1) 214-648-7084
E-mail: jinming.gao@utsouthwestern.edu
Prof. K. Luby-Phelps
Department of Cell Biology
UT Southwestern Medical Center at Dallas (USA)
Prof. B. D. Sumer
Department of Otolaryngology
UT Southwestern Medical Center at Dallas (USA)
[+] These authors contributed equally to this work.

[**] This work was supported by the NIH (R01A129011 and R21EB005394). We thank the late Prof. R. G. W. Anderson and Prof. H. Yu for helpful discussions on cell internalization studies, E. Ross and M. Evans for stopped-flow experiments, and M. Poudel for fluorescence lifetime measurements. We would like to acknowledge the assistance of the Live Cell Imaging Shared Resource at the Harold C. Simmons Cancer Center, which is supported in part by an NCI Cancer Center Support Grant, P30CA142543.

Supporting information for this article is available on the WWW under http://dx.doi.org/10.1002/anie.201100884.

The formation of micelles and their thermodynamic stability are driven by the delicate balance between the hydrophobic and hydrophilic segments.[14] Ionizable groups can act as tunable hydrophobic groups at different pH values. Amino groups have been incorporated into polymers as ionizable groups to impart pH sensitivity.[15] Herein, we introduced tertiary amines with precisely controlled hydrophobic substituents as ionizable hydrophobic blocks. Micellization dramatically sharpens the ionization transition of tertiary amines in the hydrophobic block, thus rendering fast and ultrasensitive response to changes in pH value. Nanoparticles with different transition pH values can be selectively activated in specific endocytic compartments such as early endosomes or lysosomes in human cells.

For proof of concept, we synthesized two series of block copolymers (PEO-*b*-PR, Figure 1) with tertiary amine containing (PR) and poly(ethylene oxide) (PEO) segments by atom-transfer radical polymerization (Supporting Information Table S1).[16] In the linear dialkyl series, we varied the chain length from methyl to butyl groups; in the cyclic series, we varied the ring size from five- to seven-membered rings. The two series were systematically used to adjust the pK_a values of ammonium groups (Supporting Information Table S2) and PR hydrophobicity. A pH-insensitive dye, tetramethyl rhodamine (TMR),[17] was used as a model fluorophore and conjugated to the PR block as an imaging beacon to investigate the pH-responsive properties of the system. At higher pH values, neutral PR segments self-assemble into the hydrophobic cores of micelles, thus resulting in the aggregation of fluorophores and quenching of fluorescent signals through mechanisms of Förster resonance energy transfer between TMR molecules (homo-FRET) and photoinduced electron transfer (PeT) from tertiary amines to TMR.[18] At lower pH values, PR segments become protonated and positively charged, thus leading to micelle disassembly and dramatic increase in fluorescence emission owing to the increased distance between TMR units and the decrease in PeT (Figure 1).

Fluorescent images of a series of nanoprobe solutions (Figure 2a) at different pH values illustrate a sharp fluorescence transition for each nanoprobe. Poly(ethylene oxide)-*b*-poly((dimethylamino)ethyl methacrylate) (PEO-*b*-PDMA, **1**) was used as an "always ON" control for which no micelle formation or fluorescence quenching was observed in the tested range of pH values (4.5–8.0) owing to the strong hydrophilicity of the PDMA block (see discussion below). Normalized fluorescence intensity (NFI) vs. pH curves (Figure 2b) allowed for quantitative assessment of the ultra-pH-responsive properties. NFI is calculated as the ratio $(F-F_{min})/(F_{max}-F_{min})$, where F is the fluorescence intensity of the nanoprobe at any given pH value and F_{max} and F_{min} are the maximal and minimal fluorescence intensities in the ON and OFF states, respectively. To quantify the sharpness in pH response, we evaluated $\Delta pH_{10-90\%}$, the range of pH values in which the NFI value varies from 10 to 90%, for all the pHAM nanoprobes. The sharpness values were 0.21, 0.23, 0.24, and 0.20 pH unit for nanoprobes **4**, **6**, **3**, and **7**, respectively. The small values indicate a remarkable pH sensitivity, as they represent a less than twofold change in proton concentration. In comparison, for small-molecule dyes,[19] the sharpness value is about 2 pH units (100-fold change in $[H^+]$) for the same degree of emission change, consistent with the Henderson–Hasselbalch equation.[20] In addition to the pH sharpness, we also measured the ratio of F_{max} and F_{min} ($R_F = F_{max}/F_{min}$) to quantify the fluorescence response between the ON and OFF states. The values of R_F range from 10- to 55-fold (Supporting Information, Table S2, Figure S1). Consistent with the decreased emission intensity in the micelles, data show that the excited state of TMR had a much shorter lifetime (e.g. 0.44 ns for nanoprobe **3**, Supporting Information Figure S2) in

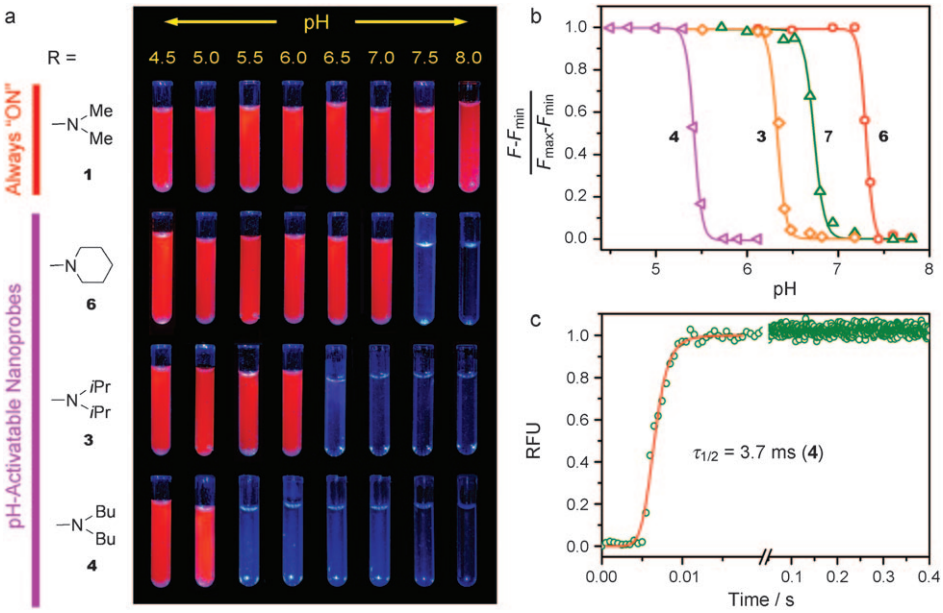

Figure 2. Illustration of tunable, ultra-pH-responsive properties of pHAM nanoprobes. a) Representative fluorescence images of different nanoprobe solutions (**6**, **3**, **4**) at the same polymer concentration (0.1 mg mL^{-1}) but different pH values. A narrow pH response is observed for each nanoprobe at different transition pH values. Copolymer **1** serves as an always "ON" control without pH response. A blue light ($\lambda_{ex} \approx 440$–480 nm, 450 mW cm^{-2}) was used to excite the nanoprobes. b) Normalized fluorescence intensity as a function of pH value for different pHAM nanoprobes. The pH response ($\Delta pH_{10-90\%}$) is less than 0.25 pH unit, and F_{max}/F_{min} is up to 55-fold (Supplementary Table S2). c) Stopped-flow fluorescence measurement of nanoprobe **4** ($pH_t = 5.4$) after activation at pH 4.9. Fluorescence recovery time ($\tau_{1/2}$) is 3.7 ms. Other pHAM nanoprobes show similarly fast kinetics (Table S2 in the Supporting Information). RFU = relative fluorescence unit.

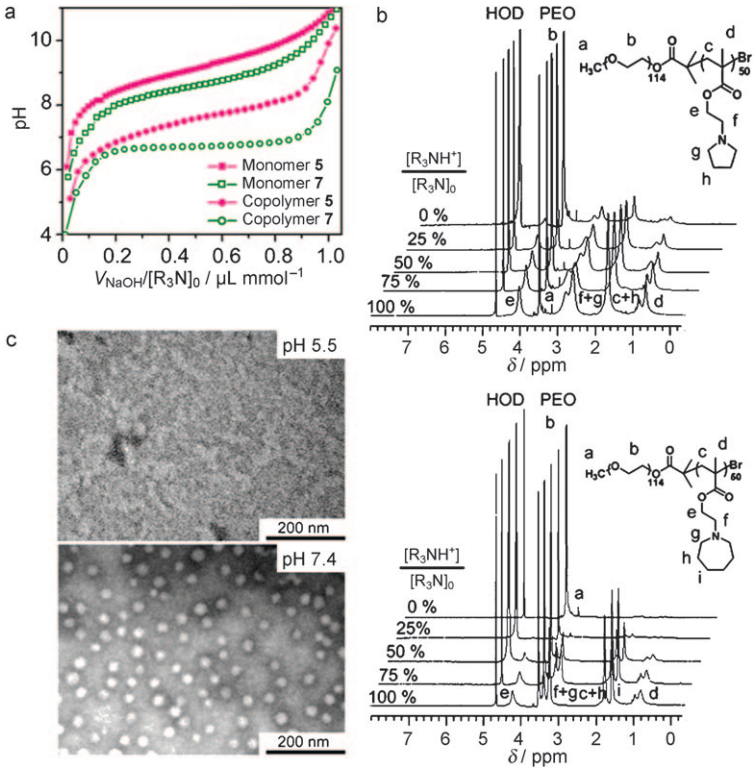

Figure 3. Investigation of the ultra-pH-responsive properties of a representative pHAM nanoprobe. a) pH titration curves of copolymers **5** and **7** and their corresponding monomers. The added volumes of NaOH (V_{NaOH}) were normalized to the initial amount of amine residues ($[R_3N]_0$ in mmol). b) ^{1}H NMR spectra (in D_2O) of **5** (top) and **7** (bottom) at different ionization states of the copolymers. c) TEM image of **7** in pH 5.5 and 7.4 buffers at a polymer concentration of 2 mg mL^{-1}.

the micelles (pH 7.4) than the free dye (1.97 ns) at pH 7.4 or the disassembled unimers at pH 5.5 (1.84 ns).

For the pH temporal response, stopped-flow experiments showed that fluorescence activation was very fast, with most nanoprobes fully activated within 5 ms at pH values lower than their respective pK_a values (e.g. $\tau_{1/2} = 3.7$ ms for **4**, Figure 2c). The ultrasensitive pH response was only observed with **4**, **3**, **7**, and **6**. The fluorescence transition pH values (pH_t, the pH value at which $F = 0.5(F_{max}+F_{min})$) were 5.4, 6.3, 6.8, and 7.2 for nanoprobes **4**, **3**, **7**, and **6**, respectively (Figure 2b). The other copolymers either did not show any pH response (e.g. **1** in Figure 2a) or only broad pH responses (e.g. **2**, **5**, data not shown). We hypothesize that hydrophobic micellization is the driving force for the ultra-pH-responsive properties of pHAM nanoparticles, and a critical threshold of hydrophobicity in the PR segment is necessary to achieve the cooperative response. To test this hypothesis, we used copolymers **5** and **7** as examples and compared their pH titration curves and those of the corresponding monomers (Figure 3a). Larger ring size (i.e. **7**) resulted in higher hydrophobicity in the PR segment owing to the extra methylene groups. Copolymer **5** showed a broad pH response, similar to both monomers over added volumes of NaOH. In contrast, copolymer **7** had a much sharper pH transition, thus demonstrating its better buffer capacity. ^{1}H NMR spectra of **5** and **7** in D_2O at different ionization states of tertiary amines further support the hypothesis (Figure 3b). The PEO segment did not change its peak intensity and was used as an internal standard. Throughout the ionization states, the proton resonance peaks for the PR segment of **5** were easily visualized, although the peak intensity decreased and the width broadened at higher pH values, reflecting the bulk aggregation of the copolymer. For **7**, the neutral state of the copolymer (i.e. 0%) led to completely suppressed resonances in the PR segment owing to the formation of highly compact micelle cores. Transmission electron microscopy (TEM) of **7** in aqueous solution demonstrated the formation of micelles at pH 7.4 (above its pK_a of 6.7) and complete micelle dissociation at pH 5.5 (Figure 3c). In comparison, no micelles were formed from **5** at either of these pH values (data not shown).

To investigate the intracellular activations of pHAM particles, we examined nanoprobe **3** in human H2009 lung cancer cells by confocal laser scanning microscopy (Figure S3 in the Supporting Information). It should be noted that nanoprobe **3** has an optimal pH transition at 6.3, which is ideally suited to the study of nanoparticle activation in early endosomes (pH 5.9–6.2).[13a,21] Because pHAM nanoprobes are "silent" at neutral pH values, we directly applied them in the culture medium and monitored the kinetics of their uptake and activation without the need to remove the medium. Right after the nanoprobe addition, neither the H2009 cells nor the medium showed an observable fluorescence signal. At 15 min, punctuate fluorescent dots appeared inside the cells. The number of fluorescent dots increased over time. The signal-to-noise ratio of the H2009 cells (SNR_{Cell}, using fluorescence intensity at time $t = 0$ as the background noise) allowed further quantification of the increased nanoprobe uptake and activation over time. At 60 min, a 31-fold increase in SNR_{Cell} ($(2.14 \pm 0.17) \times 10^3$) was observed over the medium ($SNR_{Med} = 69.3 \pm 9.1$, $P < 0.001$), where the majority of the nanoprobes were still present. Then 0.1N HCl solution was added to acidify the medium to pH 5.0, and considerable increase in fluorescence intensity in the medium background was found. A reverse trend of fluorescence contrast was observed, where SNR_{Cell} was 74% of SNR_{Med} ($P < 0.05$). These data illustrate that pHAM nanoprobes can dramatically increase the contrast sensitivity of cancer cells compared to potentially always-ON nanoprobes.

To further investigate whether different endocytic organelles can selectively activate pHAM systems, we transfected H2009 cells with green fluorescent protein (GFP)-fused Rab5a and Lamp1 biomarkers in early endosomes and late endosomes/lysosomes, respectively. Two pHAM nanoprobes (**3** and **4** with pH_t of 6.3 and 5.4, respectively) were incubated with H2009 cells, and confocal microscopy imaging was used to examine the subcellular locations of pHAM nanoprobe activation (Figure 4 and Figure S4 in the Supporting Infor-

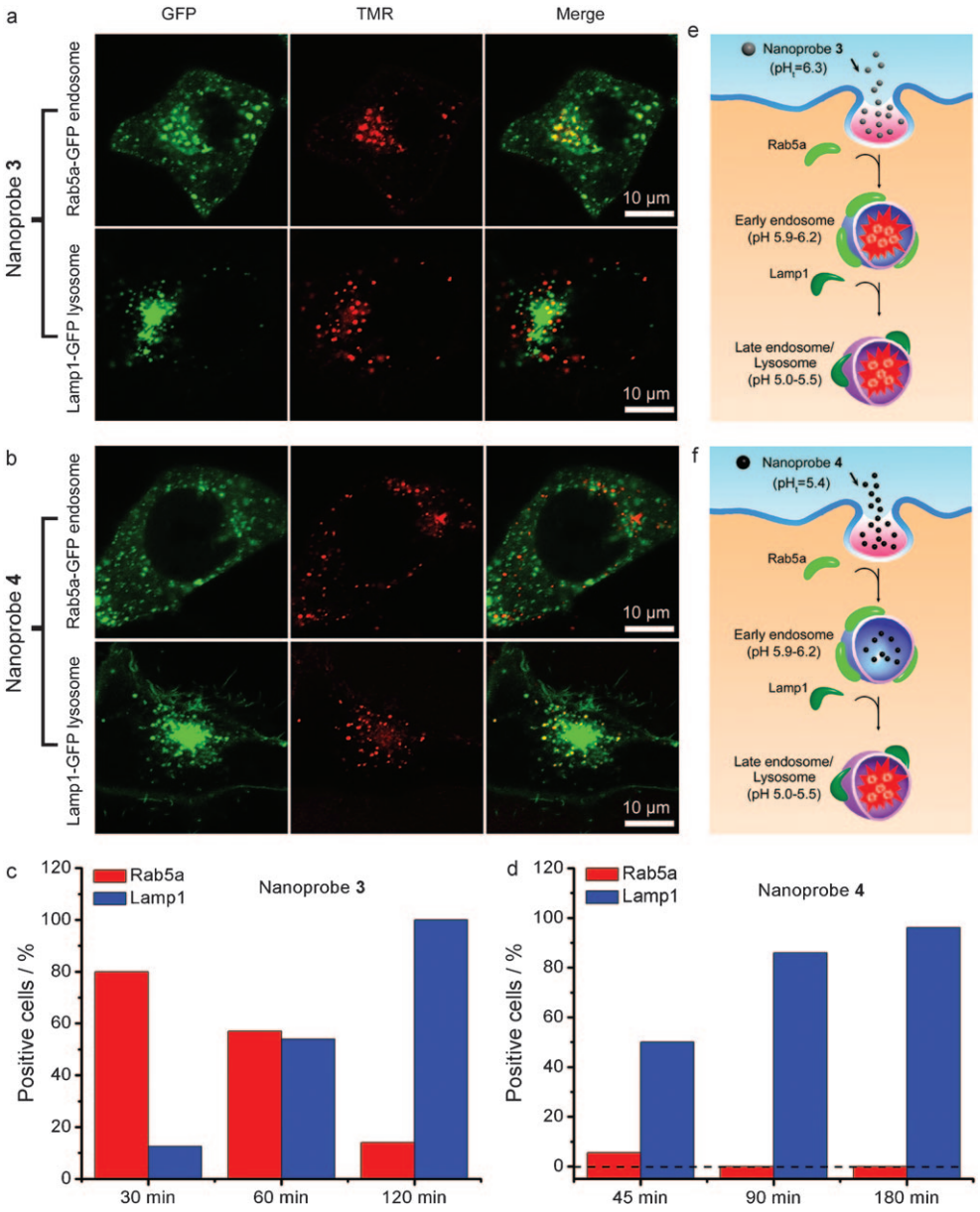

Figure 4. Investigation of subcellular activation of nanoprobes **3** and **4** in different endocytic organelles in human H2009 cells. a, b) Representative confocal microscopy images of activated nanoprobe **3** (a, $pH_t = 6.3$) and **4** (b, $pH_t = 5.4$) in cells with GFP-labeled early endosomes (top panel) and late endosomes/lysosomes (bottom panel) at 30 and 45 min, respectively. c, d) Percentage of positive cells ($N = 30$–50 cells) with activated nanoprobe **3** or **4** colocalizing with early endosomes or late endosomes/lysosomes at different incubation times. e, f) Schematic illustration of the selective activation of nanoprobe **3** in early endosomes (pH 5.9–6.2) and **4** in late endosomes/lysosomes (pH 5.0–5.5), respectively.

mation). H2009 cells ($N = 30$–50) with 20 or more colocalized dots (i.e. activated pHAM nanoprobes within early endosomes or lysosomes) were identified as positive, and the percentage was quantified (Figure 4c, d). For nanoprobe **3**, 80% of cells were positive in colocalization with early endosomes at 30 min, whereas only 12% colocalized with late endosomes/lysosomes (Figure 4a and Figure S4 in the Supporting Information). Over time, colocalization of activated **3** decreased with early endosomes but increased with late endosomes/lysosomes (Figure 4c). In contrast, nanoprobe **4** ($pH_t = 5.4$) showed a different pattern of subcellular location for activation. At all times, less than 10% of positive cells were found with early endosome colocalization (top panel of Figure 4b and Figure S4). Instead, almost all of the activated nanoprobe **4** colocalized with late endosomes/lysosomes (Figure 4b bottom panel, Figure 4d). Figure 4e, f depicts the different processes of intracellular uptake and activation of the two nanoprobes. Nanoprobe **3** can be quickly activated inside early endosomes with higher vesicular pH values (5.9–6.2),[13a,21] and the activation is sustained as the nanoprobes traffic into late endosomes/lysosomes. By contrast, nanoprobe **4** is almost exclusively activated inside the late endosomes/lysosomes with lower vesicular pH values (5.0–5.5).[13a,21] Similar results were also found with human SLK tumor endothelial cells (data not shown). These data demonstrate the feasibility of targeting small differences in the vesicular pH values inside different endocytic organelles by the pHAM nanoparticles.

To verify the intracellular activation mechanism of pHAM nanoprobes, we incubated H2009 cells with bafilomycin A1 for one hour and then added nanoprobe **3**. Bafilomycin is a specific inhibitor of vacuolar-type H^+-ATPase (V-ATPase),[22] which is responsible for the proton pumping across the plasma membranes and acidification of intracellular organelles (e.g. lysosomes). Data show that in the presence of bafilomycin A1, nanoprobe **3** was not activated, as indicated by the absence of TMR fluorescence (Figure 5a). After removal of bafilomycin A1 and **3** in the culture medium, the activation of **3** emerged with colocalization of TMR fluorescence with GFP-labeled lysosomes (Figure 5b). Similar results were also found with nanoprobe **4** in H2009 cells (Figure S5 in the Supporting Information).

In summary, we report the design of a series of pH-activatable micellar nanoparticles with tunable and ultra-

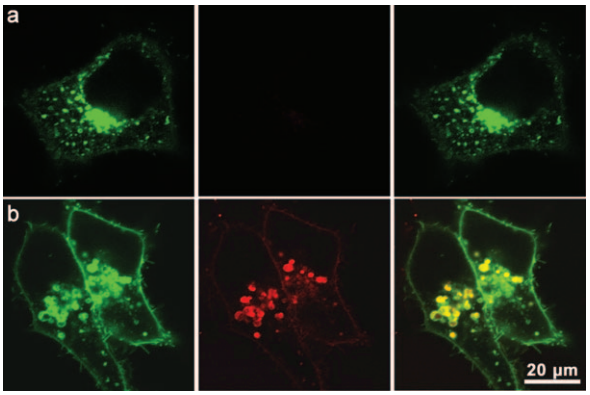

Figure 5. Inhibition of lysosomal acidification by bafilomycin A1 and its effect on intracellular activation of nanoprobe **3** in H2009 cells. a) Confocal microscopy images of cells treated with bafilomycin A1 for 1 h and subsequent incubation with nanoprobe **3** for 1 h. Lack of activation of nanoprobe **3** was observed, as demonstrated by the absence of TMR fluorescence. b) Confocal microscopy images of the same H2009 cells after removal of bafilomycin A1 and nanoprobe **3** and incubation for additional 5 h. Nanoprobe activation was observed, as indicated by the red fluorescence inside lysosomes (yellow dots in the overlay images).

sensitive pH response in the physiological range (5.0–7.4). These nanoparticles have fast temporal response (< 5 ms), large increase of emission intensity between ON and OFF states (up to 55 times), and require a change of only less than 0.25 pH units for activation. Confocal imaging studies demonstrate that the nanoparticles are "silent" in the media at pH 7.4 but can be activated upon uptake in cells. Moreover, nanoparticles with transitions at pH 6.3 and 5.4 can be selectively activated in different endocytic compartments such as early endosomes (pH 5.9–6.2) and lysosomes (5.0–5.5). This nanoplatform offers many exciting opportunities in the development of nonlinear ON/OFF nanosystems for diagnostic imaging and drug delivery applications with minimal effect at physiological pH values (e.g. pH 7.4) but can be activated at acidic tumor pH values or in specific intracellular organelles (e.g. endosomes/lysosomes) upon uptake in targeted cells.

Received: February 3, 2011
Published online: April 14, 2011

Keywords: cell cycle · fluorescent probes · micelles · nanostructures · pH activation

[1] a) S. Singhal, S. Nie, M. D. Wang, *Annu. Rev. Med.* **2010**, *61*, 359–373; b) K. Riehemann, S. W. Schneider, T. A. Luger, B. Godin, M. Ferrari, H. Fuchs, *Angew. Chem.* **2009**, *121*, 886–913; *Angew. Chem. Int. Ed.* **2009**, *48*, 872–897; c) R. Weissleder, M. J. Pittet, *Nature* **2008**, *452*, 580–589; d) M. E. Davis, Z. Chen, D. M. Shin, *Nat. Rev. Drug Discovery* **2008**, *7*, 771–782; e) D. Peer, J. M. Karp, S. Hong, O. C. Farokhzad, R. Margalit, R. Langer, *Nat. Nanotechnol.* **2007**, *2*, 751–760.

[2] a) V. Torchilin, *Eur. J. Pharm. Biopharm.* **2009**, *71*, 431–444; b) E. S. Lee, Z. G. Gao, Y. H. Bae, *J. Controlled Release* **2008**, *132*, 164–170.

[3] a) E. S. Lee, K. Na, Y. H. Bae, *J. Controlled Release* **2003**, *91*, 103–113; b) Y. Bae, S. Fukushima, A. Harada, K. Kataoka, *Angew. Chem.* **2003**, *115*, 4788–4791; *Angew. Chem. Int. Ed.* **2003**, *42*, 4640–4643; c) D. M. Lynn, M. M. Amiji, R. Langer, *Angew. Chem.* **2001**, *113*, 1757–1760; *Angew. Chem. Int. Ed.* **2001**, *40*, 1707–1710.

[4] a) S.-W. Choi, Y. Zhang, Y. Xia, *Angew. Chem.* **2010**, *122*, 8076–8080; *Angew. Chem. Int. Ed.* **2010**, *49*, 7904–7908; b) B. Jeong, Y. H. Bae, S. W. Kim, *J. Controlled Release* **2000**, *63*, 155–163.

[5] a) C. Wang, Q. Chen, Z. Wang, X. Zhang, *Angew. Chem.* **2010**, *122*, 8794–8797; *Angew. Chem. Int. Ed.* **2010**, *49*, 8612–8615; b) E. S. Olson, T. Jiang, T. A. Aguilera, Q. T. Nguyen, L. G. Ellies, M. Scadeng, R. Y. Tsien, *Proc. Natl. Acad. Sci. USA* **2010**, *107*, 4311–4316; c) A. Bernardos, E. Aznar, M. D. Marcos, R. Martínez-Máñez, F. Sancenón, J. Soto, J. M. Barat, P. Amorós, *Angew. Chem.* **2009**, *121*, 5998–6001; *Angew. Chem. Int. Ed.* **2009**, *48*, 5884–5887.

[6] a) Y.-L. Li, L. Zhu, Z. Liu, R. Cheng, F. Meng, J.-H. Cui, S.-J. Ji, Z. Zhong, *Angew. Chem.* **2009**, *121*, 10098–10102; *Angew. Chem. Int. Ed.* **2009**, *48*, 9914–9918; b) G. Saito, J. A. Swanson, K. D. Lee, *Adv. Drug Delivery Rev.* **2003**, *55*, 199–215.

[7] a) S. Febvay, D. M. Marini, A. M. Belcher, D. E. Clapham, *Nano Lett.* **2010**, *10*, 2211–2219; b) D. V. Volodkin, A. G. Skirtach, H. Mohwald, *Angew. Chem.* **2009**, *121*, 1839–1841; *Angew. Chem. Int. Ed.* **2009**, *48*, 1807–1809; c) A. G. Skirtach, A. Muñoz Javier, O. Kreft, K. Köhler, A. Piera Alberola, H. Möhwald, W. J. Parak, G. B. Sukhorukov, *Angew. Chem.* **2006**, *118*, 4728–4733; *Angew. Chem. Int. Ed.* **2006**, *45*, 4612–4617.

[8] a) R. A. Gatenby, R. J. Gillies, *Nat. Rev. Cancer* **2008**, *8*, 56–61; b) R. J. Gillies, N. Raghunand, M. L. Garcia-Martin, R. A. Gatenby, *IEEE Eng. Med. Biol. Mag.* **2004**, *23*, 57–64; c) I. F. Tannock, D. Rotin, *Cancer Res.* **1989**, *49*, 4373–4384.

[9] a) Y. Tian, F. Su, W. Weber, V. Nandakumar, B. R. Shumway, Y. Jin, X. Zhou, M. R. Holl, R. H. Johnson, D. R. Meldrum, *Biomaterials* **2010**, *31*, 7411–7422; b) J. Y. Ko, S. Park, H. Lee, H. Koo, M. S. Kim, K. Choi, I. C. Kwon, S. Y. Jeong, K. Kim, D. S. Lee, *Small* **2010**, *6*, 2539–2544; c) J.-Z. Du, T.-M. Sun, W.-J. Song, J. Wu, J. Wang, *Angew. Chem.* **2010**, *122*, 3703–3708; *Angew. Chem. Int. Ed.* **2010**, *49*, 3621–3626; d) E. S. Lee, Z. G. Gao, D. Kim, K. Park, I. C. Kwon, Y. H. Bae, *J. Controlled Release* **2008**, *129*, 228–236; e) R. M. Sawant, J. P. Hurley, S. Salmaso, A. Kale, E. Tolcheva, T. S. Levchenko, V. P. Torchilin, *Bioconjugate Chem.* **2006**, *17*, 943–949; f) E. S. Lee, K. Na, Y. H. Bae, *Nano Lett.* **2005**, *5*, 325–329.

[10] a) Y. Bae, N. Nishiyama, K. Kataoka, *Bioconjugate Chem.* **2007**, *18*, 1131–1139; b) A. Potineni, D. M. Lynn, R. Langer, M. M. Amiji, *J. Controlled Release* **2003**, *86*, 223–234; c) F. Kratz, U. Beyer, M. T. Schutte, *Crit. Rev. Ther. Drug Carrier Syst.* **1999**, *16*, 245–288.

[11] a) Z. X. Zhou, Y. Q. Shen, J. B. Tang, M. H. Fan, E. A. Van Kirk, W. J. Murdoch, M. Radosz, *Adv. Funct. Mater.* **2009**, *19*, 3580–3589; b) Y. Lee, K. Miyata, M. Oba, T. Ishii, S. Fukushima, M. Han, H. Koyama, N. Nishiyama, K. Kataoka, *Angew. Chem.* **2008**, *120*, 5241–5244; *Angew. Chem. Int. Ed.* **2008**, *47*, 5163–5166; c) Y. Lee, S. Fukushima, Y. Bae, S. Hiki, T. Ishii, K. Kataoka, *J. Am. Chem. Soc.* **2007**, *129*, 5362–5363.

[12] a) A. E. Nel, L. Madler, D. Velegol, T. Xia, E. M. V. Hoek, P. Somasundaran, F. Klaessig, V. Castranova, M. Thompson, *Nat. Mater.* **2009**, *8*, 543–557; b) D. Maysinger, *Org. Biomol. Chem.* **2007**, *5*, 2335–2342; c) P. Watson, A. T. Jones, D. J. Stephens, *Adv. Drug Delivery Rev.* **2005**, *57*, 43–61.

[13] a) J. R. Casey, S. Grinstein, J. Orlowski, *Nat. Rev. Mol. Cell Biol.* **2010**, *11*, 50–61; b) F. R. Maxfield, T. E. McGraw, *Nat. Rev. Mol. Cell Biol.* **2004**, *5*, 121–132.

[14] a) K. Zhou, Y. Lu, J. Li, L. Shen, G. Zhang, Z. Xie, C. Wu, *Macromolecules* **2008**, *41*, 8927–8931; b) G. Riess, *Prog. Polym.*

Sci. **2003**, *28*, 1107 – 1170; c) E. S. Lee, H. J. Shin, K. Na, Y. H. Bae, *J. Controlled Release* **2003**, *90*, 363 – 374.
[15] a) M. S. Kim, S. J. Hwang, J. K. Han, E. K. Choi, H. J. Park, J. S. Kim, D. S. Lee, *Macromol. Rapid Commun.* **2006**, *27*, 447 – 451; b) V. Bütün, S. P. Armes, N. C. Billingham, *Polymer* **2001**, *42*, 5993 – 6008.
[16] a) N. V. Tsarevsky, K. Matyjaszewski, *Chem. Rev.* **2007**, *107*, 2270 – 2299; b) Y. H. Ma, Y. Q. Tang, N. C. Billingham, S. P. Armes, A. L. Lewis, A. W. Lloyd, J. P. Salvage, *Macromolecules* **2003**, *36*, 3475 – 3484.
[17] L. Albertazzi, B. Storti, L. Marchetti, F. Beltram, *J. Am. Chem. Soc.* **2010**, *132*, 18158 – 18167.
[18] a) H. Kobayashi, M. Ogawa, R. Alford, P. L. Choyke, Y. Urano, *Chem. Rev.* **2010**, *110*, 2620 – 2640; b) S. Uchiyama, K. Iwai, A. P. de Silva, *Angew. Chem.* **2008**, *120*, 4745 – 4747; *Angew. Chem. Int. Ed.* **2008**, *47*, 4667 – 4669; c) J. R. Lakowicz, *Principles of Fluorescence Spectroscopy*, 3rd ed., Springer, New York City, **2006**, pp. 443 – 475; d) Y. Diaz-Fernandez, F. Foti, C. Mangano, P. Pallavicini, S. Patroni, A. Perez-Gramatges, S. Rodriguez-Calvo, *Chem. Eur. J.* **2006**, *12*, 921 – 930.
[19] Y. Urano, D. Asanuma, Y. Hama, Y. Koyama, T. Barrett, M. Kamiya, T. Nagano, T. Watanabe, A. Hasegawa, P. L. Choyke, H. Kobayashi, *Nat. Med.* **2009**, *15*, 104 – 109.
[20] P. Atkins, J. De Paula, *Physical Chemistry*, Oxford University Press, Oxford, **2009**.
[21] S. Modi, M. G. Swetha, D. Goswami, G. D. Gupta, S. Mayor, Y. Krishnan, *Nat. Nanotechnol.* **2009**, *4*, 325 – 330.
[22] S. Gagliardi, M. Rees, C. Farina, *Curr. Med. Chem.* **1999**, *6*, 1197 – 1212.

